JACS Au
AN OPEN ACCESS JOURNAL OF THE AMERICAN CHEMICAL SOCIETY

pubs.acs.org/jacsau

Article

Photocatalytic Oxidative Dehydrogenation of Propane for Selective Propene Production with TiO_2

Fangliang Li,[†] Binli Wang,[†] Xiao Chen, Yuemiao Lai, Tao Wang, Hongjun Fan,* Xueming Yang, and Qing Guo*

Cite This: *JACS Au* 2022, 2, 2607−2616

Read Online

ACCESS | Metrics & More | Article Recommendations | Supporting Information

ABSTRACT: Oxidative dehydrogenation of propane (ODHP) as an exothermic process is a promising method to produce propene (C_3H_6) with lower energy consumption in chemical industry. However, the selectivity of the C_3H_6 product is always poor because of overoxidation. Herein, the ODHP reaction into C_3H_6 on a model rutile(R)-TiO_2(110) surface at low temperature via photocatalysis has been realized successfully. The results illustrate that photocatalytic oxidative dehydrogenation of propane (C_3H_8) into C_3H_6 can occur efficiently on R-TiO_2(110) at 90 K via a stepwise manner, in which the initial C−H cleavage occurs via the hole coupled C−H bond cleavage pathway followed by a radical mediated C−H cleavage to the C_3H_6 product. An exceptional selectivity of ∼90% for C_3H_6 production is achieved at about 13% propane conversion. The mechanistic model constructed in this study not only advances our understanding of C−H bond activation but also provides a new pathway for highly selective ODHP into C_3H_6 under mild conditions.

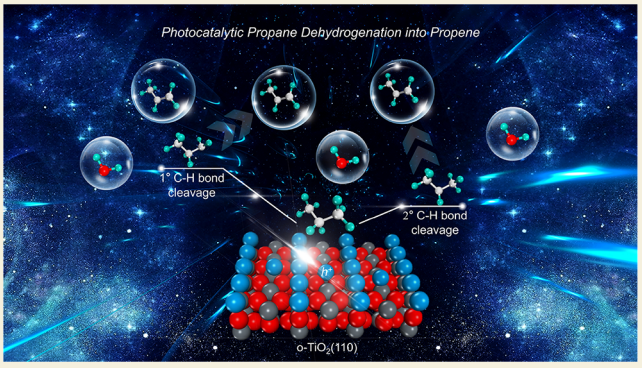

KEYWORDS: *photocatalysis, TiO_2, ODHP, propene, reaction mechanism*

INTRODUCTION

The recent large-scale exploitation of shale gas that contains abundant light alkanes has emerged as a way to effectively supplement traditional fossil fuels, such as naphtha and heavy oil.[1−3] Light olefins from the conversion of saturated alkanes are important building blocks for many chemicals, such as plastics, fibers, and oxygenates.[1−7] However, because of the stability of alkanes resulting from high symmetry, weak polarizability, and high bond energy of the sp^3 C−H bond, the commercial processes for light olefins production from alkanes are always conducted at high temperatures and pressures.[1−7] The severe reaction conditions result in a large amount of energy consumption, catalyst deactivation, environmental pollution, and safety issues.

Propane (C_3H_8) is one of the main components of shale gas, and its dehydrogenation product, propene (C_3H_6), is a very important industrial raw materials.[1−6] The ongoing discovery of shale gas leads to the development of a direct C_3H_8 dehydrogenation technology to produce C_3H_6. Thus, a lot of scientific research has also been focused on this subject.[1−6] Compared to the nonoxidative dehydrogenation of C_3H_8 (DHP) process, the oxidative dehydrogenation of C_3H_8 (ODHP) is considered as an emerging crafts for C_3H_6 production because of its thermodynamic preference and the hindrance of coke formation.[1−6] However, the ODHP process is still a highly energy-intensive process, which is usually conducted in mixed high temperature steam,[2,3,8−13] It inevitably causes the overoxidation of intermediates and products, lowering the selectivity of desired C_3H_6 product. Consequently, reducing the reaction temperature and preventing the facile overoxidation of C_3H_6 product is still the key scientific challenge for the ODHP process.

After decades of research, various catalysts have been developed for the ODHP process. Among them, emerging boron-containing catalysts (e.g., BN, supported boron oxide) can lower the reaction temperature efficiently and successfully suppress the overoxidation of olefin products to a certain extent.[2,5,14−25] Although a very high olefin molecular selectivity (C_3H_6 and ethene) can be achieved with boron-containing catalysts, a high reaction temperature (usually in excess of 400 °C) is still required.[2,5,14,15,19] However, the C_3H_6 selectivity is still not entirely satisfactory. Therefore, alternative catalysts and reaction pathways with the ability to better control undesired C−C bond cleavage and overoxidation need to be explored.

Received: September 16, 2022
Revised: October 15, 2022
Accepted: October 17, 2022
Published: October 27, 2022

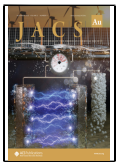

https://doi.org/10.1021/jacsau.2c00512
JACS Au 2022, 2, 2607−2616

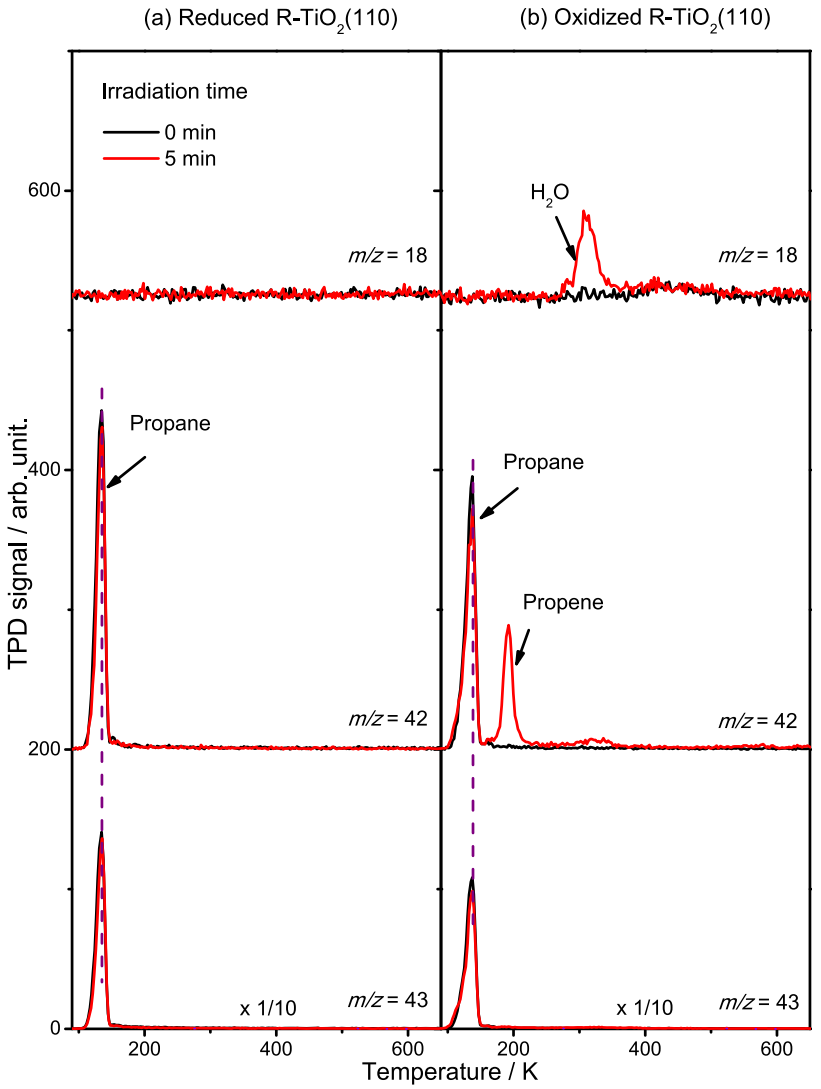

Figure 1. Typical TPD spectra acquired at m/z = 18 (H_2O^+), 42 ($C_3H_6^+$), and 43 ($C_3H_7^+$) after adsorbing 0.36 ML of C_3H_8 on the (a) reduced and (b) oxidized R-TiO_2(110) surfaces at 90 K with (5 min, red lines) and without (0 min, black lines) 355 nm irradiation. The oxidized R-TiO_2(110) surfaces were prepared by exposing reduced surfaces to 200 L of O_2 at 300 K. The photon flux of 355 nm light is 1.6×10^{16} photons cm^{-2} s^{-1}.

Photocatalysis is an emerging technology that utilizes light energy instead of high-temperature thermal energy to drive reactions under mild conditions.[26] Recently, the photocatalytic oxidative dehydrogenation of small alkanes under mild conditions was successfully achieved over TiO_2 based catalysts,[27−29] indicating that TiO_2-based photocatalysis technology may be a promising way for selective C_3H_6 production from C_3H_8 dehydrogenation under mild conditions. Herein, we report on photocatalytic ODHP to C_3H_6 on rutile(R)-TiO_2(110) via the hole coupled C−H bond cleavage process at 90 K. A high selectivity of about 90% for the C_3H_6 product is achieved at about 13% C_3H_8 conversion. Moreover, a clear mechanistic insight into photocatalytic ODHP to C_3H_6 on R-TiO_2(110) has also been provided.

RESULTS AND DISCUSSION

Figure 1 shows the typical temperature-programmed desorption (TPD) spectra of mass-to-charge ratios (m/z) of 18 (H_2O^+), 42 ($C_3H_6^+$), and 43 ($C_3H_7^+$) collected on the reduced and oxidized R-TiO_2(110) surfaces after adsorbing 0.36 ML (1 ML = 5.2×10^{14} atoms/cm^2) of C_3H_8 followed by 355 nm irradiation for 0 (black line) and 5 min (red line). The oxidized surfaces were prepared by exposing the reduced R-TiO_2(110) surfaces to 200 L of O_2 at 300 K, resulting in major adsorption of O atoms on the Ti_{5c} sites (O_{Ti}) of the surfaces and healing of the bridging oxygen vacancy sites (O_v).[30,31] Before irradiation, only one desorption peak at 137 K appears in the TPD traces of m/z = 42 and 43 on the reduced and oxidized surfaces, which is attributed to the desorption of C_3H_8 on the Ti_{5c} sites ($C_3H_{8(Ti)}$).[32] No observation of new products during the TPD process illustrates that no thermochemistry of C_3H_8 occurs on both the oxidized and reduced surfaces. Likewise, no products are detected on the C_3H_8 covered reduced R-TiO_2(110) surface after 355 nm light irradiation, indicating that reduced R-TiO_2(110) is photo-inactive for the conversion of C_3H_8.

However, two new desorption features at 190 K (m/z = 42) and 310 K (m/z = 18) are observed on the 0.36 ML C_3H_8 covered oxidized R-TiO_2(110) surface after irradiation for 5 min. Here, 190 K is determined for the desorption of C_3H_6 molecules on the Ti_{5c} sites ($C_3H_{6(Ti)}$) (Figures S1 and S2 in

https://doi.org/10.1021/jacsau.2c00512
JACS Au 2022, 2, 2607−2616

the Supporting Information, SI). The 310 K peak can be attributed to the desorption of H_2O molecules on the Ti_{5c} sites (H_2O_{Ti}) or the recombinative desorption of terminal OH groups on the Ti_{5c} sites (OH_{Ti}).[33] In addition, no recombinative desorption signal of H_2O from the OH groups on the bridging oxygen rows (OH_b)[30] suggests that H atoms produced from C_3H_8 dehydrogenation are mostly likely to be abstracted by O_{Ti} atoms directly rather than bridging oxygen atoms (O_b) during the photocatalytic process. Otherwise, the C_3H_6 product should also be detected on the reduced R-TiO_2(110) surface. To further identify the role of O_{Ti} atoms in photocatalytic ODPH on R-TiO_2(110), an isotope labeling experiment with $^{18}O_2$ was carried out. On the $^{18}O_2$ oxidized R-TiO_2(110) surfaces, only the $H_2{}^{18}O_{Ti}$ product is detected (Figure S3), illustrating that only $^{18}O_{Ti}$ atoms are involved in photocatalytic ODHP. Therefore, photocatalytic ODHP occurs on oxidized R-TiO_2(110) at 90 K following reaction 1:

$$C_3H_{8(Ti)} + O_{Ti} + h\nu \rightarrow CH_3CH{=}CH_{Ti} + H_2O_{Ti} \quad (1)$$

No obvious signals of other products (Figure S2) demonstrate that the C_3H_6 production on oxidized R-TiO_2(110) via photocatalytic ODHP takes place with high selectivity.

In addition to the selectivity of C_3H_6 product, the conversion efficiency of C_3H_8 is also important. As shown in Figure 2, the formation of C_3H_6 and H_2O products and the decay of C_3H_8 were monitored by the TPD traces of m/z = 18, 29, and 42 collected from the 0.36 ML C_3H_6 covered oxidized R-TiO_2(110) surfaces at different irradiation times. With increasing irradiation time, the $C_3H_{8(Ti)}$ peak at 137 K (m/z = 29 and 42) is gradually depleted. Concomitant to the decrease of the $C_3H_{8(Ti)}$ peak, both H_2O_{Ti} and $C_3H_{6(Ti)}$ products increase obviously and then reach saturation. A shoulder peak at 105 K appears in the TPD spectra of m/z = 29 and 42 with irradiation time, which is attributed to C_3H_8 adsorption on O_b atoms.[32] The appearance of the shoulder peak is due to the competitive adsorption between $C_3H_{8(Ti)}$ and $C_3H_{6(Ti)}$, H_2O_{Ti} products, leading to part of the less strongly adsorbed $C_3H_{8(Ti)}$ to be repelled to O_b atoms.[32] In addition, a small peak at 300 K (m/z = 29, the inset of Figure 2b) appears and increases with irradiation time, as well as the small peak at 340 K (m/z = 42, the inset of Figure 2c). Referring to the OPDH process on IrO_2(110),[34] the former may be assigned to the desorption of C_3H_8 via recombination of the C_3H_7 groups and H atoms on the surface, and the latter is likely due to the C_3H_6 product produced via thermocatalytic dehydrogenation of the C_3H_7 groups (see more details in Figure S2).

From Figure 2a and c, the yields of H_2O and C_3H_6 products on oxidized R-TiO_2(110) as a function of ultraviolet (UV) irradiation time can be obtained (Figure 3a). With increasing irradiation time, the yields of both products grow gradually and slowly reach saturation at 180 min (~0.047 ML H_2O and ~0.043 ML C_3H_6). And the selectivity of the C_3H_6 product (S_{C3H6} = yield of $C_3H_{6(Ti)}$ at 190 K/yield of H_2O at 310 K) and the conversion efficiency of C_3H_8 (X_{C3H8} = yield of H_2O at 310 K/initial coverage of C_3H_8) are also depicted in Figure 3b. As the irradiation time increases, X_{C3H8} increases rapidly and reaches a plateau (about 13%) while S_{C3H6} decreases slightly from ~95% to ~90%. Therefore, photocatalytic OPDH into C_3H_6 can be achieved on oxidized R-TiO_2(110) at 90 K with high selectivity and moderate C_3H_8 conversion efficiency. In addition, the yield of the C_3H_6 product has a quasi-linear relationship with irradiation time when the irradiation time is ≤60 s (inset of Figure 3a). The quantum yield is defined as

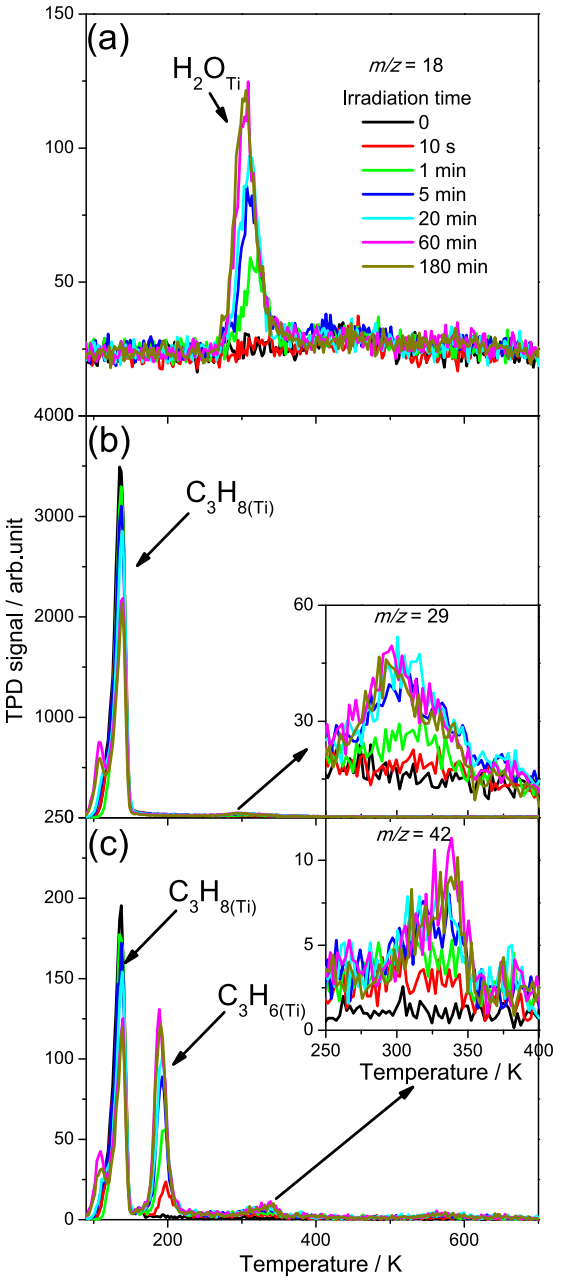

Figure 2. Typical spectra acquired at m/z = (a) 18 (H_2O^+), (b) 29 ($C_2H_5^+$), and (c) 42 ($C_3H_6^+$) on the 0.36 ML C_3H_8 covered oxidized R-TiO_2(110) surfaces as a function of irradiation time.

"yield of C_3H_8/number of incident photons"; thus, the initial quantum yield of C_3H_6 production can be roughly estimated to be 1.1×10^{-5}.

As shown in Figure 1, no observation of product signal from C_3H_8 dehydrogenation on both the reduced and oxidized R-TiO_2(110) surfaces suggests that R-TiO_2(110) has no thermocatalytic dehydrogenation ability of C_3H_8. In contrast, PdO(101), RuO_2(110), and IrO_2(110) surfaces that have strong oxidability for C_3H_8 dehydrogenation, in which the C_3H_8 molecule has a strong interaction with the substrate by forming a molecular σ-complex precursor at first and then breaks the C−H bond as the surface temperature increases.[34−40] C_3H_8 only weakly adsorbs on R-TiO_2(110), and surface oxidation does not enhance its adsorption. Therefore, even if the C−H bond activation of C_3H_8 occurs

https://doi.org/10.1021/jacsau.2c00512
JACS Au 2022, 2, 2607−2616

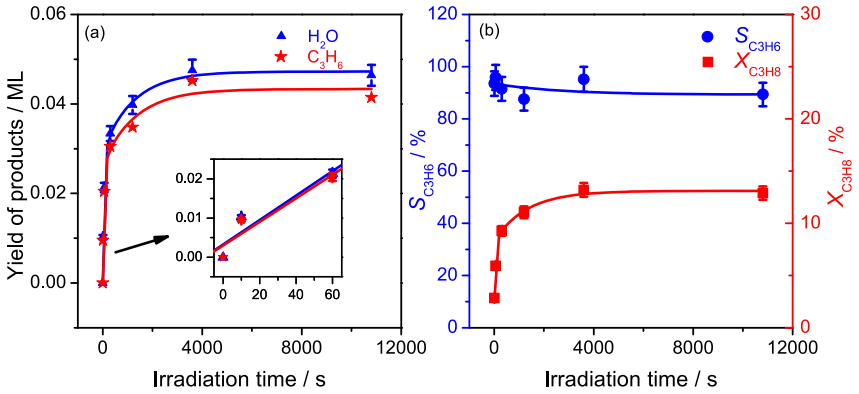

Figure 3. (a) Yields of H_2O (blue triangle) and C_3H_6 (red star), and (b) selectivity of C_3H_6 product (S_{C3H6}, blue circle) and conversion efficiency of C_3H_8 (X_{C3H8}, red square) for photocatalytic C_3H_8 dehydrogenation on oxidized R-TiO_2(110) as a function of irradiation time, obtained from Figure 2a and c. The inset of (a) shows a quasi-linear relationship between the yield of C_3H_6 product and irradiation time when the irradiation time is ≤60 s. All the plotted lines are only to guide the eye.

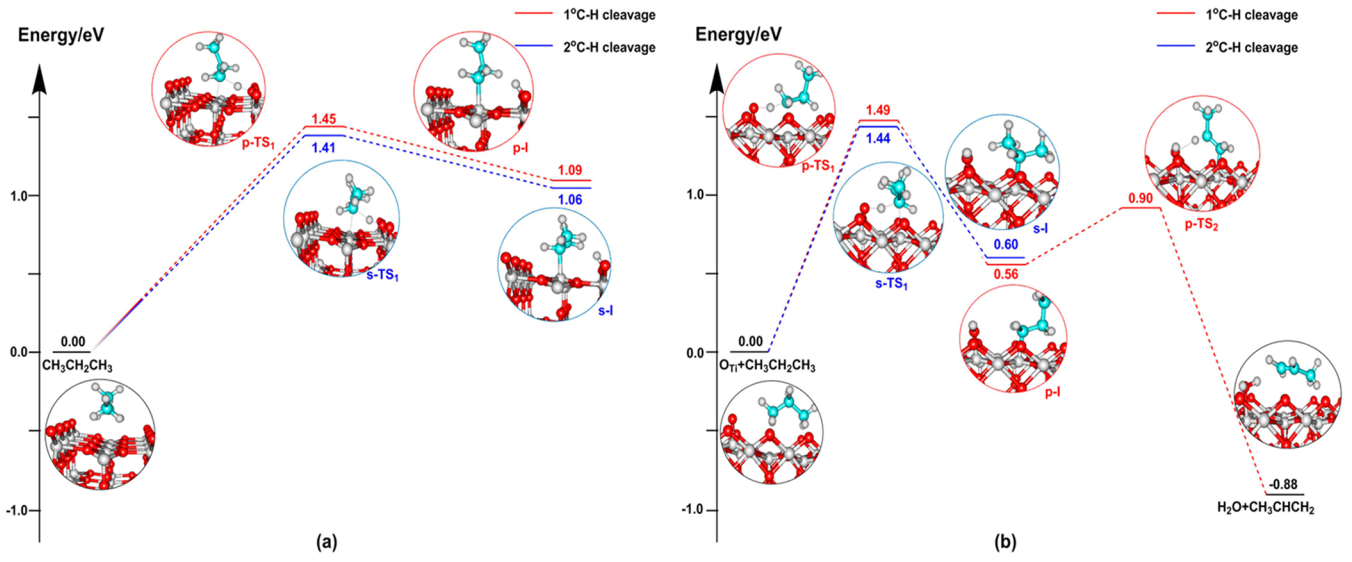

Figure 4. Energy profiles of the initial C−H cleavage of C_3H_8 on the (a) stoichiometric and (b) oxidized R-TiO_2(110) surfaces. The cleavage of the primary (1°) and secondary (2°) C−H bonds leads to a propyl group ($-CH_2CH_2CH_3^-$) and isopropyl group ($-CH_3CHCH_3^-$) intermediate, respectively. Following the 1° C−H bond cleavage pathway on the oxidized surface, the second dehydrogenation of the intermediate into C_3H_6 as a prototype is also investigated.

on R-TiO_2(110) either via thermocatalysis or photocatalysis, the weak adsorption of C_3H_8 cannot satisfy the conditions of the precursor mediated mechanism.[25]

However, photocatalytic ODHP occurs smoothly on oxidized R-TiO_2(110), indicating that the process is achieved via another mechanism. Recently, a gas-phase reaction mechanism has been proposed for photocatalytic C−H bond activation of hydrocarbons on R-TiO_2(110), where the O^- centers derived from O_b atoms under UV excitation abstract the H atoms of hydrocarbons to form corresponding radicals.[41,42] A similar gas-phase radical mechanism was also proposed in the process of ODHP of BN-based catalysts.[5,25] Here, although only O_{Ti} atoms are active species for photocatalytic ODHP on R-TiO_2(110), the underlying mechanism may be similar. Following a similar mechanism, the $C_3H_7^•$ radical will be produced first during the photocatalytic ODHP process. Then, most of the radicals will undergo further dehydrogenation into C_3H_6 directly (the dominating $C_3H_{6(Ti)}$ product at 190 K), instead of entering the gas phase like the case of methane CH_4 on R-TiO_2(110),[41] or binding to the surface via a radical-rebound process like the cases of toluene ($C_6H_5CH_3$) on R-TiO_2(110)[42] and C_3H_8 on BN catalysts.[5] Otherwise, compared with 0.047 ML H_2O production, tiny carbon-containing products should be observed, or most of the carbon-containing products should appear at high temperature (>300 K) (small peaks of C_3H_6 and C_3H_8 produced via thermal processes at >300 K, Figure S2).

To provide a more detailed mechanistic model for photocatalytic C−H bond activation in the OPDH process on R-TiO_2(110), theoretical calculations for the adsorption and photocatalytic dehydrogenation of C_3H_8 on the R-TiO_2(110) surface were performed (theoretical details are depicted in the SI). Referring to the adsorption structure of C_3H_8 on PdO(101), the p-2η^1 adsorption structure of C_3H_8 (C_3H_8 coordinating with the surface by forming two H−Pd dative bonds, one at each CH_3 group) on R-TiO_2(110) is the most stable one with an adsorption energy (E_{ads}) of 0.60 eV (Figure S4). However, the E_{ads} values of the other two structures (p-η^2, C_3H_8 binding through two H atoms of one CH_3 group, E_{ads} = 0.49 eV; s-η^2, C_3H_8 binding through two H

https://doi.org/10.1021/jacsau.2c00512
JACS Au 2022, 2, 2607−2616

atoms of the CH_2 group, E_{ads} = 0.52 eV, Figure S4) are very close to that of the p-2η^1 structure. In addition, the existence of O_{Ti} atoms has a minimal effect on the adsorption of C_3H_8 (Figure S4), in agreement with the TPD result. Thus, different from exclusive 1° C−H bond cleavage resulting from the p-2η^1 σ-complex precursor formation on PdO(101),[36] the initial C−H cleavage of 1° and 2° C−H bonds should be taken into consideration, which produces a propyl group ($-CH_2CH_2CH_3^-$) or isopropyl group ($-CH_3CHCH_3^-$) intermediate, respectively.

As shown in Figure 4, the energy profiles of the initial C−H bond activation of C_3H_8 via thermocatalysis on both the stoichiometric and oxidized R-TiO_2(110) surfaces are described. On the stoichiometric R-TiO_2(110) surface, the cleavage of the 1° C−H bond is endothermic by 1.09 eV with a barrier of 1.45 eV, and the cleavage of 2° C−H bond is endothermic by 1.06 eV with a barrier of 1.41 eV, both of which are endothermic processes with high energy barriers. After surface oxidation, the endothermal value for the initial C−H bond activation is largely reduced. The cleavage of the 1° C−H bond is endothermic by 0.56 eV with a barrier of 1.49 eV, and the cleavage of 2° C−H bond is endothermic by 0.60 eV with a barrier of 1.44 eV. However, the energy barriers of the initial C−H bond cleavage are nearly unchanged, which still far exceed the E_{ads} of $C_3H_{8(Ti)}$ (0.49−0.60 eV, Figure S4). Therefore, the initial C−H bond activation via thermocatalytic processes on both stoichiometric and oxidized R-TiO_2(110) is thermodynamically infeasible. In addition, following the 1° C−H bond cleavage pathway on the oxidized surface, further dehydrogenation of the propyl intermediate into C_3H_6 as a prototype has also been investigated, which is exothermic by 1.44 eV with an energy barrier of 0.34 eV. Thus, the initial C−H bond cleavage is the rate-determining step for the OPDH process on R-TiO_2(110), which prohibits the activation of C_3H_8 on the O_{Ti} atom covered R-TiO_2(110) surfaces thermodynamically.

By introducing a hole into the O_{Ti} atom covered R-TiO_2(110) surface, photocatalytic ODHP on R-TiO_2(110) was performed. According to recent theoretical results about C−H bond activation of CH_4 on R-TiO_2(110),[41] the C−H bond activation of CH_4 on R-TiO_2(110) under photoexcitation includes not only the energy transfer process but also the hole transfer process. Similarly, the process of hole transfer along with the 1° C−H bond cleavage pathway as a prototype is shown in the form of spin density distribution in Figure 5. The larger electron accumulation on O_{Ti} than O_b atom (Bader charge is −1.01 for O_{Ti}, while −0.87 for O_b) makes the former a better site for hole trapping. Thus, initially, the hole will be trapped by an O_{Ti} atom rather than an O_b atom (Figure 5a) due to its stronger ability of hole capture. Subsequently, the hole will be located at both the 1° C atom of C_3H_8 and the O_{Ti} atom (p-TS_1 in Figure 5b), indicating that the photocatalytic cleavage of 1° C−H bond on oxidized R-TiO_2(110) is more likely to be a homolytic process.[41,42] Because the alkyl group shows a better hole capture ability than OH_{Ti} groups,[43] the hole will be localized at the C atom of the C_3H_7 moiety to form a propyl radical after the 1° C−H bond cleavage, and the dissociated H atom transfers to an adjacent O_{Ti} atom, forming an OH_{Ti} group (Figure 5c). Likewise, the 2° C−H bond cleavage also follows the similar mechanism to form an isopropyl radical, which is no longer discussed in detail here.

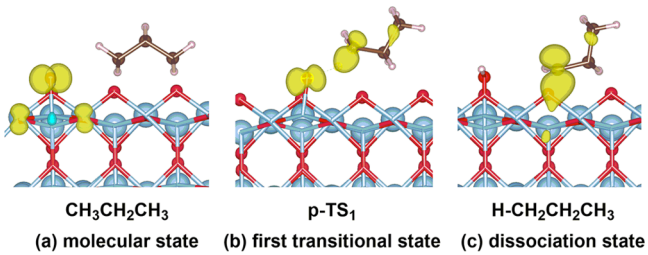

Figure 5. Spin density distribution of (a) molecular state, (b) first transition state (TS_1) and (c) dissociation state on the O_{Ti} atoms covered R-TiO_2(110) surface in the process of the 1° C−H cleavage of C_3H_8, respectively. O atoms (red), titanium atoms (blue), carbon atoms (black) and hydrogen atoms (white) are represented by small balls of different colors, respectively. The yellow area represents the spin density of electron clouds.

With these calculations, the energy profiles of photocatalytic ODHP on the O_{Ti} atom covered R-TiO_2(110) surface can be obtained (Figure 6). For the 1° C−H bond cleavage pathway, the initial 1° C−H bond cleavage of C_3H_8 to propyl radical is exothermic by 0.93 eV with a barrier of 0.53 eV. Compared with the thermocatalytic case (Figure 4), such a photocatalytic homolytic C−H cleavage is much more feasible for the formation of $CH_3CH_2C_{Ti}H_2$ radical and HO_{Ti}. Then the α-H in the propyl radical intermediate will transfer to HO_{Ti} directly to form C_3H_6 and H_2O_{Ti} easily, and this step is exothermic by 1.41 eV with an energy barrier of 0.51 eV. Similarly, for the 2° C−H bond cleavage pathway, the stepwise dehydrogenation processes are exothermic by 1.14 and 1.20 eV with the energy barriers of 0.18 and 0.22 eV, respectively. Although the latter pathway is more favorable because of the lower energy barriers for each step, the possibility of the 1° C−H bond cleavage pathway cannot be completely ruled out because of its strongly exothermic effect with moderate barriers. The two competitive pathways are more likely to occur simultaneously in a certain proportion, similar to the reaction in gas-phase systems,[44,45] rather than undergoing highly regioselective 1° or 2° C−H bond cleavage.

Generally, the thermocatalytic C−H bond activation of alkanes on high-valent metal oxo compounds usually follows the proton coupled electron transfer (PCET) mechanism.[41,46,47] For instance, on the PdO(101), RuO_2(110), and IrO_2(110) surfaces,[39,48−50] theoretical calculations proposed that the empty d_z^2 orbital of the surface metal atom (Pd, Ru, Ir) accepts the electron donated from the C−H σ-bond, accompanied by a filled d_{xy} orbital for the back-bonding to the C−H antibonding orbital, leading to the formation of C_3H_8 σ-complex on the surfaces (mainly staggered p-2η^1 complex). As a result, metal centers acted as Lewis acidic sites lower the energy barrier of C−H bond cleavage significantly, and lattice O atoms acted as Lewis basic sites extract protons via the PCET process, synergistically resulting in heterolytic C−H bond cleavage to form stable C_3H_7 groups on the surfaces at low temperature.[34−40] The weak interaction between C_3H_8 and the Ti_{5c} atom of R-TiO_2(110) inhibits the formation of the C_3H_8 σ-complex, similar to the case of CH_4 on R-TiO_2(110).[32,41,50] The thermocatalytic C−H bond activation of C_3H_8 has a high barrier (>1.0 eV, Figure 4) on both the reduced and oxidized R-TiO_2(110) surfaces, which far exceeds the E_{ads} of C_3H_8. Thus, C_3H_8 molecules prefer to desorb from the surface rather than break the C−H bonds on both the reduced and oxidized R-TiO_2(110) surfaces during the TPD

https://doi.org/10.1021/jacsau.2c00512
JACS Au 2022, 2, 2607−2616

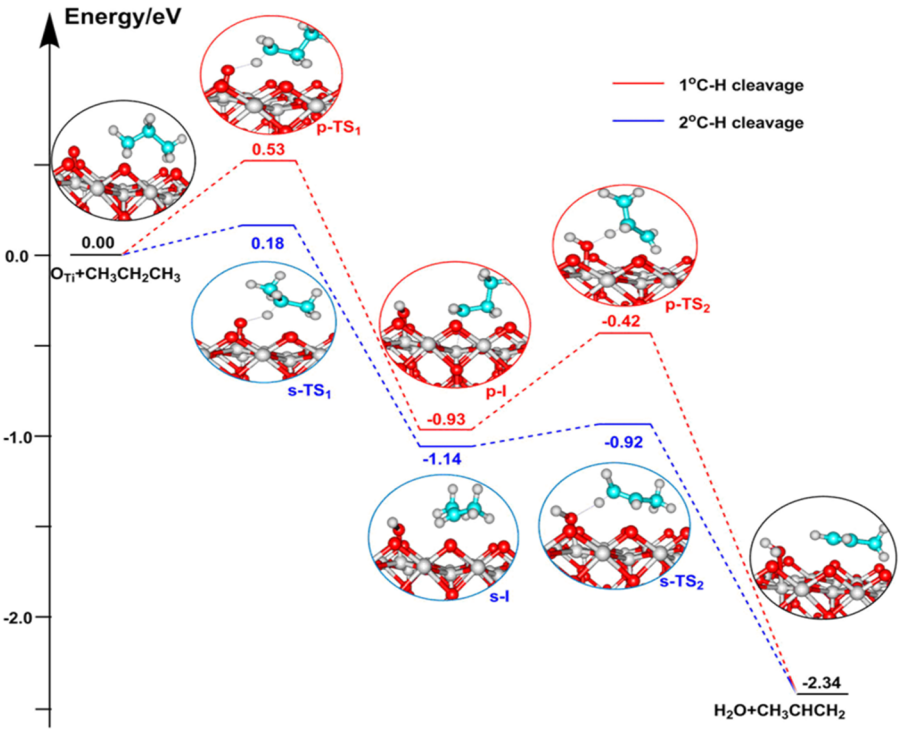

Figure 6. Energy profiles of the ODHP process on O_{Ti} atom covered R-TiO_2(110) surface under photoexcitation. The two pathways represent the initial 1° (up) and 2° (below) C−H cleavage.

process. Otherwise, different states of C_3H_8 desorption should be detected in the TPD spectra, similar to the result of C_3H_8 desorption on IrO_2(110) and RuO_2(110).[34,40]

Although the weak interaction between C_3H_8 and the Ti_{5c} atoms of R-TiO_2(110) inhibits the thermocatalytic OPDH process, photocatalytic OPDH into C_3H_6 can occur smoothly on the oxidized surface at 90 K, demonstrating that photocatalysis could alter the reaction pathway significantly. The corresponding theoretical result (Figure 6) shows that both photocatalytic 1° and 2° C−H bond cleavages of C_3H_8 are strongly exothermic processes, which have much lower energy barriers than those of the thermocatalytic processes. Because of the weak interaction between C_3H_8 and the Ti_{5c} atom, the initial C−H bond cleavage in photocatalytic OPDH on R-TiO_2(110) is unlikely to occur via the stable precursor-mediated mechanism. The theoretical result of spin density distribution (Figure 5) suggests that the photocatalytic C−H bond cleavage of C_3H_8 on oxidized R-TiO_2(110) follows a homolytic hydrogen atom transfer (HAT) mechanism to form $C_3H_7^{\bullet}$ radical rather than a heterolytic C−H bond cleavage process, which is close to the gas-phase $C_3H_7^{\bullet}$ radical formation pathway of the ODHP process.[25,51] However, the energy barriers for the initial C−H bond cleavage have a noticeable difference. In the gas phase, the homolytic bond dissociation energies are 410 kJ/mol (~4.2 eV) for the 1° C−H bond and 398 kJ/mol (~4.1 eV) for the 2° C−H bond.[36] Here, the energy barriers for photocatalytic 1° and 2° C−H bond cleavage decrease to only about 0.53 and 0.18 eV on oxidized R-TiO_2(110), respectively. Such small energy barriers imply that photocatalytic OPDH could occur efficiently on R-TiO_2(110).

Similarly, theoretical works[36] about photocatalytic CH_4 dehydrogenation on R-TiO_2(110) also proposed that the initial C−H bond activation is exothermic by 0.23 eV with a barrier of 0.29 eV and the hole trapped O_b atoms (O_b^- centers) play a crucial role in C−H bond activation. Moreover, according to the experimental work about photocatalytic C−H bond activation of toluene on reduced R-TiO_2(110),[42] O_b^- centers show a very high activity for photocatalytic C−H bond activation of toluene. Similar results of photocatalytic C−H bond activation of small alkanes with the assistance of O^- centers on different surfaces have also been observed.[52,53] Unlike direct dissociative adsorption resulted from strong interactions between C_3H_8 and IrO_2(110),[34] photocatalytic ODHP on R-TiO_2(110) follows the oxygen-mediated Eley−Rideal adsorption pathway,[25] in which O atoms are preabsorbed and C_3H_8 weakly adsorbs and facilely migrates on the surface. The dehydrogenation reaction is likely to occur when mobile C_3H_8 molecules efficiently collide with reactive O_{Ti}^- centers.

Because the C_3H_8 molecule is less symmetrical and more polar than CH_4, the C−H bond activation of C_3H_8 with the O_b^- center should be much easier than CH_4 on R-TiO_2(110) theoretically. However, the C−H bond activation of C_3H_8 is only detected on the oxidized R-TiO_2(110) surface, in which the hole trapped O_{Ti} atom (O_{Ti}^- center) plays an important role in C−H bond cleavage (Figure 5). The big difference between theoretical predictions and experimental results may be attributed to two possible reasons. First, although both O_b^- and O_{Ti}^- can be generated as active sites under UV light irradiation, O_b^- can only activate the active α-H of toluene[42] but cannot activate the inert C−H bond of C_3H_8. This suggests that the dehydrogenation ability of the O_{Ti}^- center may be stronger than that of the O_b^- center. In addition, the observation of the reversible switch between O_{Ti}^{2-} and O_{Ti}^- by a combination of noncontact atomic force microscopy (nc-AFM) and Kelvin probe force microscopy (KPFS) at 78 K[54−57] indicates that O_{Ti}^- is likely a long-lived species on R-

https://doi.org/10.1021/jacsau.2c00512
JACS Au 2022, 2, 2607−2616

TiO_2(110) at low surface temperature, which will be suitable for low-temperature photocatalytic ODHP.

Thus, once O_{Ti}^- centers are formed on R-TiO_2(110) via trapping photogenerated holes, the abstraction of a H atom from C_3H_8 by the hole trapped O_{Ti}^- center can occur to produce the $C_3H_7^\bullet$ radical (propyl radicals or isopropyl radicals) via the HAT process (Figure 5). According to the work on photocatalytic C−H bond activation of toluene on R-TiO_2(110),[42] the formation of stable benzyl intermediates (or benzyl anions) via a radical rebound process during the UV irradiation process will result in an obvious recombination peak of toluene in the TPD spectra. In other words, R-TiO_2(110) may act as a radical quenching agent, similar to the role of hexagonal boron nitride (h-BN) catalysts in the ODHP process.[58] However, only a tiny recombination peak for C_3H_8 is observed in Figure 2, which is likely due to the recombination of stable C_3H_7 groups and H_b atoms.[34,40] The tiny recombinative desorption peak of C_3H_8 demonstrates that dissociated $C_3H_7^\bullet$ radicals prefer to dehydrogenate into C_3H_6 rather than convert into stable C_3H_7 groups, which is due to the low energy barrier of the second C−H bond cleavage (especially 2° C−H cleavage, 0.22 eV in Figure 6), leading to efficient C_3H_6 production.

Recently, Hermans et al. also obtained a high olefin selectivity (79% C_3H_6 and 12% ethene) over h-BN and boron nitride nanotubes (BNNTs).[5] They proposed that the high olefin selectivity is largely enhanced due to the rebound step of the $C_3H_7^\bullet$ radical on the nitroxyl-radical site, avoiding the ejection of $C_3H_7^\bullet$ radical into gas phase or the migration of $C_3H_7^\bullet$ radical on the surface for further reaction with oxidant, then resulting in a high selectivity of C_3H_6 product.[5] For ODHP on R-TiO_2(110), the C−Ti bond between the C_3H_7 intermediate ($C_3H_7^-$) and the Ti_{5c} site on the O_{Ti} atom covered surface is 2.09 Å after the heterolytic C−H bond cleavage (Figure S5). However, upon 355 nm irradiation, the C−Ti bond between the hole-trapped $C_3H_7^\bullet$ radical and the Ti_{5c} site is 2.76 Å, suggesting that $C_3H_7^\bullet$ radicals physically adsorb on R-TiO_2(110), similar to the case on Ga_2O_3(100).[59] When the hole-trapped $C_3H_7^\bullet$ radical rebounds to the R-TiO_2(110) surface via a de-excitation process as in the case of toluene,[42] the stable C_3H_7 intermediate will be formed. The small recombinative desorption peak of C_3H_8 at >300 K (Figure S2) suggests that the rebound step of the $C_3H_7^\bullet$ radical is just a minor channel. Otherwise, a big desorption peak will be detected, similar to that of photocatalytic C−H bond activation of $C_6H_5CH_3$ on R-TiO_2(110).[42] Therefore, once $C_3H_7^\bullet$ radicals are produced via photocatalytic C−H bond activation of C_3H_8 on R-TiO_2(110), the radicals will preferentially dehydrogenate into C_3H_6 rather than rebound to the surface, which is different from thermocatalytic C_3H_8 dehydrogenation on h-BN and boron nitride nanotubes.[5]

In addition, according to previous STM results, after exposing the reduced R-TiO_2(110) surface to 200 L O_2 at 300 K, the concentration of O_{Ti} atoms is almost the same as that of O_v (about 5%). As a result, O_{Ti} atoms are highly dispersed on Ti rows.[30,31] As shown in Figure 6, the DFT results indicate that both the initial and second dehydrogenation are strongly facilitated by the isolated O_{Ti}^- center, resulting in efficient ODHP into C_3H_6. In contrast, in the thermocatalytic dehydrogenation reaction of hydrocarbons, fully exposed metal clusters (e.g., Pd_3,[60] Pt_3,[61,62] $Pd_{4.4}$,[63] and so on) can simultaneously balance the adsorption of the reactants, the activation of C−H bonds, and the desorption of olefins via the synergy of adjacent sites, resulting in olefin formation with extremely high yield and selectivity. However, highly dispersed single-atom sites catalysts (SACs) encounter low catalytic efficiency and sintering due to the lack of synergistically successive dehydrogenation from neighboring sites. Therefore, although the efficiency of photocatalysis is less than that of thermocatalysis, it is a promising technology for hydrocarbon dehydrogenation with low energy consumption and possibly high atom-utilization in the future.

CONCLUSIONS

In summary, model studies of photocatalytic ODHP on R-TiO_2(110) demonstrates that the process can occur on the R-TiO_2(110) surface with an exceptional selectivity of >90% for C_3H_6 production. Further mechanistic analysis determines that O_{Ti}^- centers rather than O_b^- centers produced via trapping photogenerated holes play a vital role in the initial C−H bond activation of C_3H_8 via the HAT process, resulting in the high selectivity of C_3H_6 production at low surface temperature. The findings not only provide a novel mechanistic insight into photocatalytic C−H bond activation by means of the experiment and the theory, but also offer new opportunities for the rational design of highly selective ODHP pathways under mild conditions.

METHODS

Experimental Section

All TPD experiments were performed with a home-built apparatus, which has been described in detail elsewhere.[64] The preparation of well-ordered R-TiO_2(110) crystal surfaces (Princeton Scientific Corp., 10 mm × 10 mm × 1 mm) was accomplished by cycles of Ar^+ sputtering and annealing at 850 K in ultrahigh vacuum (UHV). The characterization of the ordering and cleanness of the R-TiO_2(110) surfaces was conducted by low-energy electron diffraction (LEED) and Auger electron spectroscopy (AES), respectively. The density of O_v on the surface was determined by about 5%, as gauged by H_2O TPD. The purity of the C_3H_8, O_2, and isotopic O_2^{18} gas used in the experiment was 99.99%. The 355 nm light was produced by the third harmonic output from a diode pumped, solid state (DPSS), Q-switched 1064 nm laser (Spectra-Physics). The pulse time and repetition rate of the UV laser were 12 ns and 50 kHz, respectively. The power of the laser was only 5 mW with a flux of about 1.6×10^{16} photons cm^{-2} s^{-1}, and the increase of surface temperature resulting from laser irradiation can be ignored.

Computational Section

Theoretical calculations were performed with the Vienna ab initio simulation package (VASP) code[65,66] and plane augmented wave potential.[67] The wave function was expanded by the plane wave, with a basis cutoff of 400 eV. The spin-polarized Perdew−Burke−Ernzerhof functional[68] was used. Van der Walls correction (DFT-D3)[69] was applied for the dispersion interactions. The constrained minimization and climbing-image nudged elastic band methods (CI-NEB)[70] were used to search the transition states and calculate the energy barriers. The Bader charge was applied to analyze the charge distribution.

The surface model was cut out of a TiO_2 crystal to expose the (110) surface, with a six-layer slab and 4 × 2 surface unit cell. A 15 Å vacuum region was used to decouple the surface slab. A Monkhorst−Pack grid[71] of (1 × 1 × 1) k-point mesh was used in the calculations.

The C−H bond cleavage on three kinds of R-TiO_2(110) surfaces were included: stoichiometric surface, oxidized surface, and photo-excited oxidized surface. The oxidized surface was simulated with an O_{Ti} atom on the top of the slab and two H atoms adsorbed on the bridge oxygen (HO_b) on the bottom of the slab, which were applied to neutralize the unpaired electrons. According to previous studies, a

https://doi.org/10.1021/jacsau.2c00512
JACS Au 2022, 2, 2607−2616

hydroxyl can be used as an electron-withdrawing group to inject a hole to the surface.[72−74] Similarly, an O_{Ti} atom on the top of the slab and a HO_b on the bottom of the slab were used to introduce a photogenerated hole to the oxidized surface in the simulation.

■ ASSOCIATED CONTENT

Supporting Information

The Supporting Information is available free of charge at https://pubs.acs.org/doi/10.1021/jacsau.2c00512.

Typical spectra acquired at m/z = 39 ($C_3H_3^+$), 40 ($C_3H_4^+$), 41 ($C_3H_5^+$), and 42 ($C_3H_6^+$) on the 0.40 ML C_3H_6 covered R-TiO_2(110) surface; typical spectra acquired at different masses on the 0.36 ML C_3H_8 covered oxidized R-TiO_2(110) surfaces followed by irradiating the surface for 0 and 5 min at 90 K, respectively; TPD traces of different masses collected on the 0.36 ML C_3H_8 covered R-TiO_2(110) surfaces oxidized by $^{18}O_2$ at 300 K followed by irradiating the surface for 0 and 5 min at 90 K; different adsorption configurations and adsorption energy of C_3H_8 on the stoichiometric and oxidized R-TiO_2(110) surface; adsorption structure of dissociated C_3H_7 intermediate; and C−Ti bond and distance calculated with a van der Waals correction (PDF)

■ AUTHOR INFORMATION

Corresponding Authors

Hongjun Fan − *State Key Laboratory of Molecular Reaction Dynamics, Dalian Institute of Chemical Physics, Chinese Academy of Sciences, Dalian, Liaoning 116023, P. R. China;* orcid.org/0000-0003-3406-6932; Email: fanhj@dicp.ac.cn

Qing Guo − *Shenzhen Key Laboratory of Energy Chemistry & Department of Chemistry, Southern University of Science and Technology, Shenzhen, Guangdong 518055, P. R. China;* orcid.org/0000-0001-7029-3978; Email: guoq@sustech.edu.cn

Authors

Fangliang Li − *Shenzhen Key Laboratory of Energy Chemistry & Department of Chemistry, Southern University of Science and Technology, Shenzhen, Guangdong 518055, P. R. China;* orcid.org/0000-0002-0189-7564

Binli Wang − *Shenzhen Institute of Advanced Technology, Chinese Academy of Sciences, Shenzhen, Guangdong 518055, P. R. China;* orcid.org/0000-0002-1906-0762

Xiao Chen − *Shenzhen Key Laboratory of Energy Chemistry & Department of Chemistry, Southern University of Science and Technology, Shenzhen, Guangdong 518055, P. R. China;* orcid.org/0000-0002-1356-7917

Yuemiao Lai − *Shenzhen Key Laboratory of Energy Chemistry & Department of Chemistry, Southern University of Science and Technology, Shenzhen, Guangdong 518055, P. R. China;* orcid.org/0000-0002-4622-8225

Tao Wang − *Shenzhen Key Laboratory of Energy Chemistry & Department of Chemistry, Southern University of Science and Technology, Shenzhen, Guangdong 518055, P. R. China;* orcid.org/0000-0002-6091-1020

Xueming Yang − *Shenzhen Key Laboratory of Energy Chemistry & Department of Chemistry, Southern University of Science and Technology, Shenzhen, Guangdong 518055, P. R. China; State Key Laboratory of Molecular Reaction Dynamics, Dalian Institute of Chemical Physics, Chinese Academy of Sciences, Dalian, Liaoning 116023, P. R. China; Hefei National Laboratory, Hefei 230088, P. R. China;* orcid.org/0000-0001-6684-9187

Complete contact information is available at: https://pubs.acs.org/10.1021/jacsau.2c00512

Author Contributions

†F.L. and B.W. contributed equally to this work.

Notes

The authors declare no competing financial interest.

■ ACKNOWLEDGMENTS

This work was supported by the National Key R&D Program of China (Grant No. 2018YFE0203002), the National Natural Science Foundation of China (Grant No. 22173041, 22103033, 22103031, 22173042, 21973037, NSFC Center for Chemical Dynamics), the Strategic Priority Research Program of Chinese Academy of Sciences (Grant No. XDB17000000), the Shenzhen Science and Technology Innovation Committee (Grant No. JCYJ2019080914021660, ZDSYS20200421111001787), the Guangdong Innovative & Entrepreneurial Research Team Program (Grant No. 2019ZT08L455, 2019JC01X091), the International Partnership Program of Chinese Academy of Science (Grant No. 121421KYSB20170012), and Innovation Program for Quantum Science and Technology (Grant No. 2021ZD0303304).

■ REFERENCES

(1) Dai, Y.; Gao, X.; Wang, Q.; Wan, X.; Zhou, C.; Yang, Y. Recent Progress in Heterogeneous Metal and Metal Oxide Catalysts for Direct Dehydrogenation of Ethane and Propane. *Chem. Soc. Rev.* **2021**, *50*, 5590−5630.

(2) Chen, S.; Chang, X.; Sun, G.; Zhang, T.; Xu, Y.; Wang, Y.; Pei, C.; Gong, J. Propane Dehydrogenation: Catalyst Development, New Chemistry, and Emerging Technologies. *Chem. Soc. Rev.* **2021**, *50*, 3315−3354.

(3) Zhou, H.; Yi, X.; Hui, Y.; Wang, L.; Chen, W.; Qin, Y.; Wang, M.; Ma, J.; Chu, X.; Wang, Y.; et al. Isolated Boron in Zeolite for Oxidative Dehydrogenation of Propane. *Science* **2021**, *372*, 76−80.

(4) Sattler, J. J. H. B.; Ruiz-Martinez, J.; Santillan-Jimenez, E.; Weckhuysen, B. M. Catalytic Dehydrogenation of Light Alkanes on Metals and Metal Oxides. *Chem. Rev.* **2014**, *114*, 10613−10653.

(5) Grant, J. T.; Carrero, C. A.; Goeltl, F.; Venagas, J.; Mueller, P.; Burt, S. P.; Specht, S. E.; McDermott, W. P.; Chieregato, A.; Hermans, I. Selective Oxidative Dehydrogenation of Propane to Propene Using Boron Nitride Catalysts. *Science* **2016**, *354*, 1570−1573.

(6) Wang, Y.; Hu, P.; Yang, J.; Zhu, Y. A.; Chen, D. C-H Bond Activation in Light Alkanes: A Theoretical Perspective. *Chem. Soc. Rev.* **2021**, *50*, 4299−4358.

(7) Chu, M.; Tu, W.; Yang, S.; Zhang, C.; Li, Q.; Zhang, Q.; Chen, J. Sustainable Chemical Upcycling of Waste Polyolefins by Heterogeneous Catalysis. *SusMat* **2022**, *2*, 161−185.

(8) Korzyński, M. D.; Dincă, M. Oxidative Dehydrogenation of Propane in the Realm of Metal-organic Frameworks. *ACS Cent. Sci.* **2017**, *3*, 10−12.

(9) Cavani, F.; Ballarini, N.; Cericola, A. Oxidative Dehydrogenation of Ethane and Propane: How Far from Commercial Implementation? *Catal. Today* **2007**, *127*, 113−131.

(10) Leveles, L.; Fuchs, S.; Seshan, K.; Lercher, J. A.; Lefferts, L. Oxidative Conversion of Light Alkanes to Olefins over Alkali Promoted Oxide Catalysts. *Appl. Catal., A* **2002**, *227*, 287−297.

(11) Leveles, L.; Seshan, K.; Lercher, J. A.; Lefferts, L. Oxidative Conversion of Propane over Lithium-promoted Magnesia Catalyst: I. Kinetics and Mechanism. *J. Catal.* **2003**, *218*, 296−306.
(12) Wang, S.; Du, S.; Tang, W.; Hoang, S.; Lu, X.; Xiao, W.; Zhang, B.; Weng, J.; Schneer, E.; Guo, Y.; et al. Mesoporous Perovskite Nanotube-array Enhanced Metallic-state Platinum Dispersion for Low Temperature Propane Oxidation. *ChemCatChem.* **2018**, *10*, 2184−2189.
(13) Atanga, M. A.; Rezaei, F.; Jawad, A.; Fitch, M.; Rownaghi, A. A. Oxidative Dehydrogenation of Propane to Propylene with Carbon Dioxide. *Appl. Catal., B* **2018**, *220*, 429−445.
(14) Tian, J.; Tan, J.; Xu, M.; Zhang, Z.; Wan, S.; Wang, S.; Lin, J.; Wang, Y. Propane Oxidative Dehydrogenation over Highly Selective Hexagonal Boron Nitride Catalysts: The Role of Oxidative Coupling of Methyl. *Sci. Adv.* **2019**, *5*, No. eaav8063.
(15) Lu, W. D.; Wang, D.; Zhao, Z.; Song, W.; Li, W. C.; Lu, A. H. Supported Boron Oxide Catalysts for Selective and Low-temperature Oxidative Dehydrogenation of Propane. *ACS Catal.* **2019**, *9*, 8263−8270.
(16) Qiu, B.; Jiang, F.; Lu, W. D.; Yan, B.; Li, W. C.; Zhao, Z. C.; Lu, A. H. Oxidative Dehydrogenation of Propane Using Layered Borosilicate Zeolite as the Active and Selective Catalyst. *J. Catal.* **2020**, *385*, 176−182.
(17) Venegas, J. M.; McDermott, W. P.; Hermans, I. Serendipity in Catalysis Research: Boron-Based Materials for Alkane Oxidative Dehydrogenation. *Acc. Chem. Res.* **2018**, *51*, 2556−2564.
(18) Loiland, J. A.; Zhao, Z.; Patel, A.; Hazin, P. Boron-Containing Catalysts for the Oxidative Dehydrogenation of Ethane/Propane Mixtures. *Ind. Eng. Chem. Res.* **2019**, *58*, 2170−2180.
(19) Shi, L.; Wang, D.; Song, W.; Shao, D.; Zhang, W. P.; Lu, A. H. Edge-Hydroxylated Boron Nitride for Oxidative Dehydrogenation of Propane to Propylene. *ChemCatChem.* **2017**, *9*, 1788−1793.
(20) Shi, L.; Yan, B.; Shao, D.; Jiang, F.; Wang, D.; Lu, A. H. Selective Oxidative Dehydrogenation of Ethane to Ethylene over a Hydroxylated Boron Nitride Catalyst. *Chin. J. Catal.* **2017**, *38*, 389−395.
(21) Huang, R.; Zhang, B.; Wang, J.; Wu, K. H.; Shi, W.; Zhang, Y.; Liu, Y.; Zheng, A.; Schlögl, R.; Su, D. S. Direct Insight into Ethane Oxidative Dehydrogenation over Boron Nitrides. *ChemCatChem.* **2017**, *9*, 3293−3297.
(22) Zhou, Y.; Lin, J.; Li, L.; Pan, X.; Sun, X.; Wang, X. Enhanced Performance of Boron Nitride Catalysts with Induction Period for the Oxidative Dehydrogenation of Ethane to Ethylene. *J. Catal.* **2018**, *365*, 14−23.
(23) Chaturbedy, P.; Ahamed, M.; Eswaramoorthy, M. Oxidative Dehydrogenation of Propane over a High Surface Area Boron Nitride Catalyst: Exceptional Selectivity for Olefins at High Conversion. *ACS omega* **2018**, *3*, 369−374.
(24) Tian, J.; Lin, J.; Xu, M.; Wan, S.; Lin, J.; Wang, Y. Hexagonal Boron Nitride Catalyst in a Fixed-bed Reactor for Exothermic Propane Oxidation Dehydrogenation. *Chem. Eng. Sci.* **2018**, *186*, 142−151.
(25) Kraus, P.; Lindstedt, R. P. It's a Gas: Oxidative Dehydrogenation of Propane over Boron Nitride Catalysts. *J. Phys. Chem. C* **2021**, *125*, 5623−5634.
(26) Zhang, C.; Kang, Q.; Chu, M.; He, L.; Chen, J. Solar-driven Catalytic Plastic Upcycling. *Trends Chem.* **2022**, *4*, 822−834.
(27) Xie, J.; Jin, R.; Li, A.; Bi, Y.; Ruan, Q.; Deng, Y.; Zhang, Y.; Yao, S.; Sankar, G.; Ma, D.; et al. Highly Selective Oxidation of Methane to Methanol at Ambient Conditions by Titanium Dioxide-Supported Iron Species. *Nat. Catal.* **2018**, *1*, 889−896.
(28) Zhang, R.; Wang, H.; Tang, S.; Liu, C.; Dong, F.; Yue, H.; Liang, B. Photocatalytic Oxidative Dehydrogenation of Ethane Using CO_2 as a Soft Oxidant over Pd/TiO_2 Catalysts to C_2H_4 and Syngas. *ACS Catal.* **2018**, *8*, 9280−9286.
(29) Kang, L.; Liu, X. Y.; Wang, A.; Li, L.; Ren, Y.; Li, X.; Pan, X.; Li, Y.; Zong, X.; Liu, H.; et al. Photo-thermo Catalytic Oxidation over a TiO_2-WO_3-Supported Platinum Catalyst. *Angew. Chem., Int. Ed.* **2020**, *132*, 13009−13016.
(30) Lira, E.; Hansen, J. Ø.; Huo, P.; Bechstein, R.; Galliker, P.; Lægsgaard, E.; Hammer, B.; Wendt, S.; Besenbacher, F. Dissociative and Molecular Oxygen Chemisorption Channels on Reduced Rutile TiO_2(110): An STM and TPD study. *Surf. Sci.* **2010**, *604*, 1945−1960.
(31) Sokolović, I.; Reticcioli, M.; Calkovsky, M.; Wagner, M.; Schmid, M.; Franchini, C.; Diebold, U.; Setvin, M. Resolving the Adsorption of Molecular O_2 on the Rutile TiO_2(110) Surface by Noncontact Atomic Force Microscopy. *Proc. Natl. Acad. Sci. U. S. A.* **2020**, *117*, 14827−14837.
(32) Chen, L.; Smith, R. S.; Kay, B. D.; Dohnálek, Z. Adsorption of Small Hydrocarbons on Rutile TiO_2(110). *Surf. Sci.* **2016**, *650*, 83−92.
(33) Henderson, M. A.; Epling, W. S.; Peden, C. H.; Perkins, C. L. Insights into Photoexcited Electron Scavenging Processes on TiO_2 Obtained from Studies of the Reaction of O_2 with OH Groups Adsorbed at Electronic Defects on TiO_2(110). *J. Phys. Chem. B* **2003**, *107*, 534−545.
(34) Martin, R.; Kim, M.; Franklin, A.; Bian, Y.; Asthagiri, A.; Weaver, J. F. Adsorption and Oxidation of Propane and Cyclopropane on IrO_2(110). *Phys. Chem. Chem. Phys.* **2018**, *20*, 29264−29273.
(35) Weaver, J. F.; Devarajan, S. P.; Hakanoglu, C. Facile C-H Bond Cleavage and Deep Oxidation of Propane on a PdO(101) Thin Film. *J. Phys. Chem. C* **2009**, *113*, 9773−9782.
(36) Weaver, J. F.; Hakanoglu, C.; Antony, A.; Asthagiri, A. High Selectivity for Primary C-H Bond Cleavage of Propane σ-Complexes on the PdO(101) Surface. *J. Am. Chem. Soc.* **2011**, *133*, 16196−16200.
(37) Antony, A.; Asthagiri, A.; Weaver, J. F. Pathways for C-H Bond Cleavage of Propane σ-Complexes on PdO(101). *Phys. Chem. Chem. Phys.* **2012**, *14*, 12202−12212.
(38) Zhang, F.; Pan, L.; Choi, J.; Mehar, V.; Diulus, J. T.; Asthagiri, A.; Weaver, J. F. Propane σ-Complexes on PdO(101): Spectroscopic Evidence of the Selective Coordination and Activation of Primary C-H Bonds. *Angew. Chem., Int. Ed.* **2015**, *54*, 13907−13911.
(39) Weaver, J. F.; Hakanoglu, C.; Antony, A.; Asthagiri, A. Alkane Activation on Crystalline Metal Oxide Surfaces. *Chem. Soc. Rev.* **2014**, *43*, 7536−7547.
(40) Li, T.; Kim, M.; Rai, R.; Liang, Z.; Asthagiri, A.; Weaver, J. F. Adsorption of Alkanes on Stoichiometric and Oxygen-rich RuO_2(110). *Phys. Chem. Chem. Phys.* **2016**, *18*, 22647−22660.
(41) Zhou, M.; Wang, H. Optimally Selecting Photo-and Electrocatalysis to Facilitate CH_4 Activation on TiO_2(110) Surface: Localized Photoexcitation versus Global Electric-Field Polarization. *JACS Au* **2022**, *2*, 188−196.
(42) Li, F.; Wang, B.; Chen, X.; Zeng, W.; Sun, R.; Liu, X.; Ren, Z.; Yang, X.; Fang, H.; Guo, Q. Photocatalytic C-H bond activation of toluene on rutile TiO_2(110). *J. Phys. Chem. C* **2022**, *126*, 11963−11970.
(43) Wang, B.; Wang, R.; Fan, H. Photocatalytic Activity and Hole-Scavenging Behaviors on Rutile TiO_2(100) Surfaces: A Theoretical Study. *J. Phys. Chem. C* **2022**, *126*, 974−985.
(44) Roithová, J.; Schröder, D. Gas-phase Models for Catalysis: Alkane Activation and Olefin Epoxidation by the Triatomic Cation Ag_2O^+. *J. Am. Chem. Soc.* **2007**, *129*, 15311−15318.
(45) Roithova, J.; Schroder, D. Selective Activation of Alkanes by Gas-phase Metal Ions. *Chem. Rev.* **2010**, *110*, 1170−1211.
(46) Li, J.; Zhou, S.; Zhang, J.; Schlangen, M.; Weiske, T.; Usharani, D.; Shaik, S.; Schwarz, H. Electronic Origins of the Variable Efficiency of Room-Temperature Methane Activation by Homo-and Heteronuclear Cluster Oxide Cations $[XYO_2]$+(X, Y= Al, Si, Mg): Competition between Proton-Coupled Electron Transfer and Hydrogen-Atom Transfer. *J. Am. Chem. Soc.* **2016**, *138*, 7973−7981.
(47) Fu, G.; Xu, X.; Lu, X.; Wan, H. Mechanisms of Initial Propane Activation on Molybdenum Oxides: A Density Functional Theory Study. *J. Phys. Chem. B* **2005**, *109*, 6416−6421.
(48) Fung, V.; Tao, F. F.; Jiang, D. E. Low-temperature Activation of Methane on Doped Single Atoms: Descriptor and Prediction. *Phys. Chem. Chem. Phys.* **2018**, *20*, 22909−22914.

https://doi.org/10.1021/jacsau.2c00512
JACS Au 2022, 2, 2607−2616

(49) Fung, V.; Hu, G.; Tao, F.; Jiang, D. E. Methane Chemisorption on Oxide-Supported Pt Single Atom. *ChemPhysChem* **2019**, *20*, 2217−2220.
(50) Wang, C. C.; Siao, S. S.; Jiang, J. C. C-H Bond Activation of Methane via σ-d Interaction on the $IrO_2(110)$ Surface: Density Functional Theory Study. *J. Phys. Chem. C* **2012**, *116*, 6367−6370.
(51) You, R.; Zhang, X.; Luo, L.; Pan, Y.; Pan, H.; Yang, J.; Yang, J.; Wu, L.; Zheng, X.; Jin, Y.; et al. NbO_x/CeO_2-rods Catalysts for Oxidative Dehydrogenation of Propane: Nb-CeO_2 Interaction and Reaction Mechanism. *J. Catal.* **2017**, *348*, 189−199.
(52) Ito, T.; Tashiro, T.; Watanabe, T.; Kawasaki, M.; Toi, K.; Kobayashi, H. Adsorption of Methane on Magnesium Oxide Surfaces under Ultraviolet Irradiation. *J. Chem. Soc., Faraday Trans.* **1990**, *86*, 4071−4075.
(53) Zhu, H.; Rosenfeld, D. C.; Harb, M.; Anjum, D. H.; Hedhili, M. N.; Ould-Chikh, S.; Basset, J. M. Ni-M-O (M= Sn, Ti, W) Catalysts Prepared by a Dry Mixing Method for Oxidative Dehydrogenation of Ethane. *ACS Catal.* **2016**, *6*, 2852−2866.
(54) Adachi, Y.; Wen, H. F.; Zhang, Q.; Miyazaki, M.; Sugawara, Y.; Sang, H.; Brndiar, J.; Kantorovich, L.; Štich, I.; Li, Y. J. Tip-Induced Control of Charge and Molecular Bonding of Oxygen Atoms on the Rutile $TiO_2(110)$ Surface with Atomic Force Microscopy. *ACS Nano* **2019**, *13*, 6917−6924.
(55) Adachi, Y.; Sugawara, Y.; Li, Y. J. Remotely Controlling the Charge State of Oxygen Adatoms on a Rutile $TiO_2(110)$ Surface Using Atomic Force Microscopy. *J. Phys. Chem. C* **2020**, *124*, 12010−12015.
(56) Adachi, Y.; Wen, H. F.; Zhang, Q.; Miyazaki, M.; Sugawara, Y.; Brndiar, J.; Kantorovich, L.; Štich, I.; Li, Y. J. Charge State Tristability of Oxygen Adatom on a Rutile $TiO_2(110)$-(1×1) Surface Controlled by Atomic Force Microscopy. *J. Phys. Chem. C* **2022**, *126*, 5064−5069.
(57) Zhang, Q.; Li, Y. J.; Wen, H. F.; Adachi, Y.; Miyazaki, M.; Sugawara, Y.; Xu, R.; Cheng, Z.; Brndiar, J.; Kantorovich, L.; et al. Measurement and Manipulation of the Charge State of an Adsorbed Oxygen Adatom on the Rutile $TiO_2(110)$-1×1 Surface by nc-AFM and KPFM. *J. Am. Chem. Soc.* **2018**, *140*, 15668−15674.
(58) Venegas, J. M.; Zhang, Z.; Agbi, T. O.; McDermott, W. P.; Alexandrova, A.; Hermans, I. Why Boron Nitride Is Such a Selective Catalyst for the Oxidative Dehydrogenation of Propane. *Angew. Chem., Int. Ed.* **2020**, *59*, 16527−16535.
(59) Liu, Y.; Li, Z. H.; Lu, J.; Fan, K. N. Periodic Density Functional Theory Study of Propane Dehydrogenation over Perfect $Ga_2O_3(100)$ Surface. *J. Phys. Chem. C* **2008**, *112*, 20382−20392.
(60) Wang, L.; Diao, J.; Peng, M.; Chen, Y.; Cai, X.; Deng, Y.; Huang, F.; Qin, X.; Xiao, D.; Jiang, Z.; et al. Cooperative Sites in Fully Exposed Pd Clusters for Low-temperature Direct Dehydrogenation Reaction. *ACS Catal.* **2021**, *11*, 11469−11477.
(61) Chen, X.; Peng, M.; Cai, X.; Chen, Y.; Jia, Z.; Deng, Y.; Mei, B.; Jiang, Z.; Xiao, D.; Wen, X.; et al. Regulating Coordination Number in Atomically Dispersed Pt Species on Defect-rich Graphene for n-Butane Dehydrogenation Reaction. *Nat. Commun.* **2021**, *12*, 1−9.
(62) Zhang, J.; Deng, Y.; Cai, X.; Chen, Y.; Peng, M.; Jia, Z.; Jiang, Z.; Ren, P.; Yao, S.; Xie, J.; et al. Tin-assisted Fully Exposed Platinum Clusters Stabilized on Defect-rich Graphene for Dehydrogenation Reaction. *ACS Catal.* **2019**, *9*, 5998−6005.
(63) Dong, C.; Gao, Z.; Li, Y.; Peng, M.; Wang, M.; Xu, Y.; Li, C.; Xu, M.; Deng, Y.; Qin, X.; et al. Fully Exposed Palladium Cluster Catalysts Enable Hydrogen Production from Nitrogen Heterocycles. *Nat. Catal.* **2022**, *5*, 485−493.
(64) Ren, Z.; Guo, Q.; Xu, C. B.; Yang, W.; Xiao, C.; Dai, D.; Yang, X. Surface Photocatalysis-TPD Spectrometer for Photochemical Kinetics. Chin. *J. Chem. Phys.* **2012**, *25*, 507−512.
(65) Kresse, G.; Furthmuller, J. Efficiency of Ab-Initio Total Energy Calculations for Metals and Semiconductors Using a Plane-Wave Basis Set. *Comput. Mater. Sci.* **1996**, *6*, 15−50.
(66) Kresse, G.; Furthmuller, J. Efficient Iterative Schemes for Ab-Initio Total-Energy Calculations Using a Plane-Wave Basis Set. *Phys. Rev. B* **1996**, *54*, 11169−11186.
(67) Blöchl, P. E. Projector Augmented-Wave Method. *Phys. Rev. B* **1994**, *50*, 17953.
(68) Perdew, J. P.; Burke, K.; Ernzerhof, M. Generalized Gradient Approximation Made Simple. *Phys. Rev. Lett.* **1996**, *77*, 3865−3868.
(69) Grimme, S.; Ehrlich, S.; Goerigk, L. Effect of the Damping Function in Dispersion Corrected Density Functional Theory. *J. Comput. Chem.* **2011**, *32*, 1456−1465.
(70) Henkelman, G.; Jonsson, H. Improved Tangent Estimate in the Nudged Elastic Band Method for Finding Minimum Energy Paths and Saddle Points. *J. Chem. Phys.* **2000**, *113*, 9978−9985.
(71) Monkhorst, H. J.; Pack, J. D. Special Points for Brillouin-Zone Integrations. *Phys. Rev. B* **1976**, *13*, 5188.
(72) Ji, Y.; Wang, B.; Luo, Y. GGA+U Study on the Mechanism of Photodecomposition of Water Adsorbed on Rutile $TiO_2(110)$ Surface: Free vs Trapped Hole. *J. Phys. Chem. C* **2014**, *118*, 1027−1034.
(73) Wang, D.; Wang, H.; Hu, P. Identifying the Distinct Features of Geometric Structures for Hole Trapping to Generate Radicals on Rutile $TiO_2(110)$ in Photooxidation Using Density Functional Theory Calculations with Hybrid Functional. *Phys. Chem. Chem. Phys.* **2015**, *17*, 1549−55.
(74) Zhang, J.; Peng, C.; Wang, H.; Hu, P. Identifying the Role of Photogenerated Holes in Photocatalytic Methanol Dissociation on Rutile $TiO_2(110)$. *ACS Catal.* **2017**, *7*, 2374−2380.

https://doi.org/10.1021/jacsau.2c00512
JACS Au 2022, 2, 2607−2616